Phonon dynamics of lanthanum manganite $LaMnO_3$ using an interatomic shell model potential

E. G. Rini,[1] Mala N. Rao,[2] S. L. Chaplot,[2] N. K. Gaur,[1] and R. K. Singh[3]
[1]*Department of Physics, Barkatullah University, Bhopal 462026, India*
[2]*Solid State Physics Division, Bhabha Atomic Research Centre, Mumbai 400085, India*
[3]*Centre for Basic, Applied and Nano-Sciences, Lakshmi Narain College of Technology, Bhopal 462021, India*
(Received 7 August 2006; revised manuscript received 14 December 2006; published 1 June 2007)

We have investigated the detailed phonon dynamics of the magnetoresistant lanthanum manganite ($LaMnO_3$) using a shell model with pairwise interionic interaction potential. The investigations include the computation of the phonon density of states, the specific heat, the elastic constants, and the phonon-dispersion curves of $LaMnO_3$. The symmetry vectors obtained through detailed group-theoretical analysis at the zone center point were employed to classify the phonon frequencies obtained into their irreducible representations. This analysis enabled direct comparison with the observed Raman and infrared spectra. Furthermore, we have computed the specific heat at constant volume at different temperatures and the phonon-dispersion curves along the three major symmetry directions for $LaMnO_3$. The results have been found to present an overall better interpretation of the available experimental data as compared to those obtained from other theoretical model calculations.

DOI: 10.1103/PhysRevB.75.214301 PACS number(s): 63.20.Dj, 63.20.Kr, 78.30.Hv

I. INTRODUCTION

The orthorhombic perovskites $RMnO_3$ (R = La, Y, Pr, Nd, Eu, Gd) have recently attracted intense attention as it is found that a partial substitution of R by Ca, Sr, Ba, Na, or Pb causes the phase transition and the occurrence of colossal magnetoresistance near the temperature of spin ordering of Mn ions.[1–6] These properties make these compounds promising for the magnetic sensors and the read head technology.[7] The parent compound $RMnO_3$ exhibits rich and interesting physical properties because of the strong interplay between lattice distortions, transport properties, and magnetic ordering. This compound also has a very rich phase diagram, depending on the effects of doping concentration, temperature, and pressure, being either an antiferromagnetic insulator, ferromagnetic metal, or charge-ordered insulator. One of the main ingredients of the magnetoresistance physics is the large electron-phonon interaction, enhanced by the strong Jahn-Teller character[8] of Mn^{3+} ions. Also, the thermodynamics plays an important role in describing the behavior of manganites, as many properties are attributed to the electron-phonon interaction. Thus, the study of the phonon dynamics of this material may be taken as a starting point for the consistent understanding of more complex physical properties of the doped compounds.

The crystal structure of $LaMnO_3$ has been studied using x-ray and neutron-diffraction techniques, both at ambient temperature and pressure.[9–15] Below ~800 K, $LaMnO_3$ was found to have an orthorhombic structure[15] (*Pnma* space group). The specific-heat measurements[16(a),16(b)] have been reported in the temperature range $70 \leqslant T \leqslant 760$ K using sensitive calorimeter. The Raman[17(a),17(b)] and infrared[18] experimental data have been reported for $LaMnO_3$ at room temperature and ambient pressure.

In the process of development of new and novel materials,[19–22] an important input is the fundamental understanding of the thermodynamic properties in terms of the microscopic structure and dynamics. Therefore, we have performed the detailed lattice dynamical calculations of $LaMnO_3$ using a shell model[23] with seven parameters and involving interatomic potential consisting of the long-range Coulomb and the short-range interaction terms. Earlier calculations[24–27] have employed more complex lattice dynamical models, while we have used simpler and improved model. We have investigated the phonon-dispersion curves, phonon density of states, the elastic constants, and the specific-heat of $LaMnO_3$ using the shell model.[23] Earlier, the rigid-ion model has been used by some of us[28–31] for successful description of the lattice dynamics and cohesion of molecular calcite crystals,[28] monovalent metal nitrates,[29,30] and divalent metal carbonates.[31] We have also done the group-theoretical analysis for *Pnma* space group. The symmetry vectors obtained through the detailed group-theoretical analysis along the zone center (Γ) point were employed to classify the phonon frequencies obtained into their irreducible representations. This analysis enabled us to make a direct comparison with the observed Raman[17(a),17(b)] and infrared[18] data. Also, we have computed the phonon-dispersion curves for $LaMnO_3$ along three major symmetry (Σ, Δ, and Λ) directions as assigned from the detailed group-theoretical analysis.

II. PHONON DYNAMICS AND THERMODYNAMICAL PROPERTIES

The lanthanum manganite $LaMnO_3$ (space-group *Pnma*) has an orthorhombic unit cell and four f.u./unit cell.[9,15] It has five atoms in the asymmetric unit with La and O occupying crystallographic sites 4(c), except for one oxygen atom, which is at the general position 8(d) and Mn is at 4(a) position. This structure contains a network of corner sharing MnO_6 octahedra and belongs to the family of rotationally distorted perovskites with Glazer's notation ($a^-b^+a^-$). It can be obtained from the simple perovskite structure by two consequent rotations of MnO_6 octahedra, namely, (i) around the [010] direction of cubic perovskite (y axis in *Pnma*) and (ii)

TABLE I. Comparison between the experimental (at 14 K) and calculated structural parameters (at 0 K). For the space-group *Pnma*, La, Mn, O1, and O2 atoms are located at $(x,0.25,z)$, (0,0,0), $(x,0.25,z)$, and (x,y,z), respectively, and their symmetry equivalent positions.

		a (Å)	b (Å)	c (Å)	V (Å^3)
Expt.[a]		5.739	7.672	5.532	243.580
Calc.		5.616	7.789	5.503	240.718
Calc.[b]		5.929	8.117	5.845	281.295
			x	y	z
La	Expt.[a]		0.549	0.250	0.008
	Calc.		0.541	0.250	0.007
	Calc.[b]		0.538	0.250	0.004
O1	Expt.[a]		0.487	0.250	0.575
	Calc.		0.476	0.250	0.577
	Calc.[b]		0.488	0.250	0.560
O2	Expt.[a]		0.307	0.038	0.226
	Calc.		0.292	0.041	0.206
	Calc.[b]		0.304	0.031	0.226

[a]Reference 14.
[b]Reference 24.

around the [101] direction of cubic perovskite (x axis in *Pnma*).[25] The structure has two oxygen ions O1 and O2 with different site symmetry. O1 ion lies in the symmetry plane. In *Pnma* space group, the La and O1 atoms have the site symmetry C_s. The site symmetry of Mn ion is C_i and that of O2 is C_1.[26]

We have carried out the phonon dynamical calculations using the shell model.[23] The interatomic potential includes the long-range Coulomb and short-range interactions as given by[32–34]

$$V(r) = \left(\frac{e^2}{4\pi\varepsilon_0}\right)\left[\frac{Z(k)Z(k')}{r}\right] + a\exp\left[\frac{-br}{R(k)+R(k')}\right], \tag{1}$$

where $a=1822$ eV and $b=12.364$. $Z(k)$ and $R(k)$ are the effective charge and radius parameters associated with atom k. The polarizability of the oxygen ions was modeled using the shell model, where a massless shell is linked to the core by the harmonic interactions.

We determine the parameters of the potential such that the forces on each atom and the internal stress in the crystal vanish, and it reproduces the structure close to that determined by diffraction experiments at zero pressure. Further, this potential satisfies the condition of dynamical equilibrium, and the long-wavelength phonon modes are close to their experimental values. The condition of dynamical equilibrium is that all the calculated phonon frequencies are real at all the wave vectors in the Brillouin zone. The calculations were performed using the computer program DISPR (Ref. 32) and the following optimized parameters: Z (Mn)=1.62, Z (La)=1.68, Z (O)=−1.1, R (Mn)=1.0801 Å, R (La)=1.7474 Å, R (O)=1.7976 Å, oxygen shell charge=−2.24e, and shell-core force constant=142 eV/Å^2. It was observed that the introduction of the ionic types O1 and O2 (i.e., explicitly taking into account the nonequivalent symmetry of the O ions) enables a better comparison of the calculated crystal structure to the experimentally determined structure, but does not make much difference to the values of the computed phonon frequencies. The equilibrium structure at the minimum of the potential energy thus obtained[35] has been used in the calculation of phonon-dispersion curves using the interatomic potential, as given by Eq. (1).

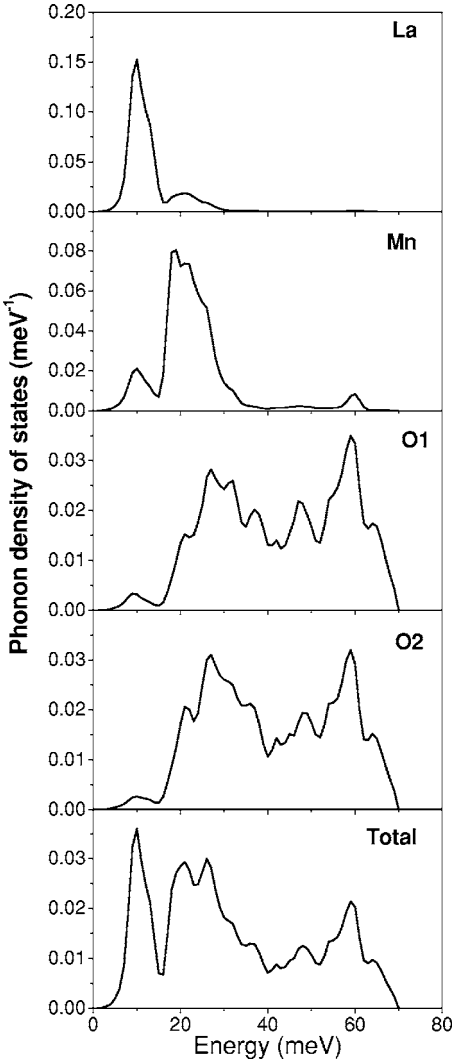

FIG. 1. The calculated partial density of states for the various atoms and the total one-phonon density of states for $LaMnO_3$. All of the spectra have been normalized to unity (1 meV=8.059 cm^{-1} =0.242 THz).

The phonon density of states is expressed as[34]

$$g(\omega) = N\int_{BZ}\sum_j \delta[\omega-\omega_j(q)]dq, \tag{2}$$

with N as a normalization constant such that $\int g(\omega)d\omega=1$, and $g(\omega)d\omega$ is the ratio of the number of eigenstates in the

TABLE II. Elastic constants (GPa) of $LaMnO_3$.

	C_{11}	C_{22}	C_{33}	C_{44}	C_{55}	C_{66}
Expt.[a]		140				
Calc.	186	157	197	72	38	77

[a]Reference 37.

frequency interval $(\omega, \omega+d\omega)$ to the total number of eigenstates. Here, $\omega_j(q)$ is the phonon frequency of the jth normal mode of the phonon wave vector q.

The calculated density of states has been used to evaluate the specific heat at constant volume $C_v(T)$ at different temperatures (T) by using the expression[33]

$$C_v(T) = k_B \int \left(\frac{\hbar\omega}{k_B T}\right)^2 \frac{e^{(\hbar\omega/k_B T)}}{[e^{(\hbar\omega/k_B T)} - 1]^2} g(\omega) d\omega. \quad (3)$$

Here, k_B is the Boltzmann constant, h is Planck's constant, and the other terms are as already defined earlier.[33] The procedures adopted for the computation of these lattice and thermodynamical properties have been discussed in detail elsewhere.[32–34]

III. GROUP-THEORETICAL ANALYSIS

We have performed detailed group-theoretical analysis of the phonon modes. For lanthanum manganite, the phonon modes at the zone center (Γ) point can be classified as

$$7A_g + 5B_{1g} + 7B_{2g} + 5B_{3g} + 10B_{1u} + 8B_{2u} + 10B_{3u} + 8A_u.$$

Of the total 60 Γ-point phonon modes, 24 $(7A_g+5B_{1g}+7B_{2g}+5B_{3g})$ are Raman active, 25 $(9B_{1u}+7B_{2u}+9B_{3u})$ are infrared active, 8 $(8A_u)$ are silent, and 3 $(B_{1u}+B_{2u}+B_{3u})$ are acoustic modes. The group-theoretical classification along the three high-symmetry directions is obtained as follows:

$$\Sigma: 17\Sigma_1 + 13\Sigma_2 + 17\Sigma_3 + 13\Sigma_4,$$

$$\Delta: 15\ \Delta_1 + 15\Delta_2 + 15\Delta_3 + 15\Delta_4,$$

$$\Lambda: 17\Lambda_1 + 13\Lambda_2 + 13\Lambda_3 + 17\Lambda_4.$$

Using this group-theoretical information, the dynamical matrix was diagonalized along three high-symmetry directions and the normal modes were classified into different representations to give the phonon-dispersion relations in $LaMnO_3$. The results obtained from the computations carried out in Secs. II and III are presented and discussed below.

IV. RESULTS AND DISCUSSION

A. Crystal structure

The calculated cell parameters and atomic coordinates of the lanthanum manganite are given in Table I and compared with the available experimental neutron-diffraction data.[9,15] The computed values of lattice parameters as well as fractional coordinates are in fairly good agreement with their experimental data.[9,15] The calculated lattice parameters differ by less than 1.5% on an average from the experimentally determined data at room temperature, similar to our earlier studies on $YBa_2Cu_3O_{7-\delta}$,[36(a)] $MgSiO_3$ perovskite,[36(b)] and the fluoroscheelites $LiYF_4$ and $LiYbF_4$.[36(c)] Describing the structural properties of complex perovskites such as $LaMnO_3$ using interatomic potentials is nontrivial, and we believe that the agreement from our calculations is satisfactory. This implies that predominantly ionic interactions are sufficient to reproduce the structure of $LaMnO_3$.

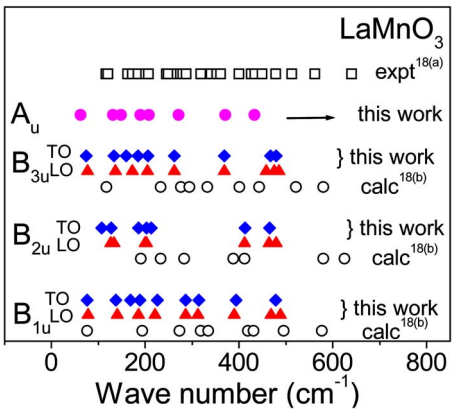

FIG. 2. (Color online) Comparison of the calculated (filled symbols—this work; open circles [Ref. 18(b)]) long-wavelength (infrared active and silent) phonon frequencies and mode assignments with available experimental data [Ref. 18(a)] (open squares). Since the experimental data are from a polycrystalline sample, a group theoretical representation-wise comparison with calculated values is not possible. The LO modes (red/gray triangles) and TO modes (blue/dark gray diamonds) (as calculated in the present work) are shown separately. The B_{1u}, B_{2u}, and B_{3u} modes are infrared active while the A_u modes are silent (1 meV=8.059 cm^{-1} =0.242 THz).

B. Elastic constants

We have calculated the elastic constants for $LaMnO_3$ through a computation of the acoustic wave velocities along different directions and depicted them in Table II. We have compared C_{22} with the experimental data available for it. As per our knowledge, there is no other experimental data on

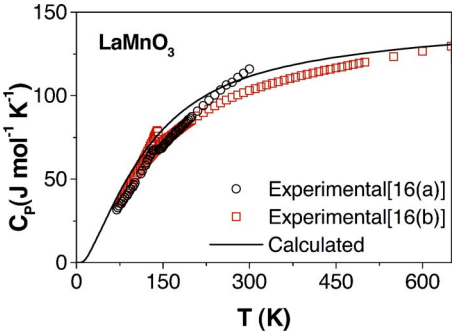

FIG. 3. (Color online) Specific heat of $LaMnO_3$ as a function of temperature. The solid line is the present model calculation. The hollow circles and hollow (red/gray) squares show data from Refs. 16(a) and 16(b), respectively.

TABLE III. Comparison of the calculated values of Raman-active phonon frequencies (in cm^{-1}) for $LaMnO_3$ with the experimental Raman data from Refs. 17(a) and 17(b). Frequencies as reported in Ref. 24 are also shown (1 meV=8.059 cm^{-1} =0.242 THz).

Expt.[a] (Raman data)	Expt.[b] (Raman data)	Calculated shell (this work)	Calculated shell[c]
	A_g		
		74	
	96	99	89
140	142	153	154
198	210	203	193
257	260	232	225
284	291	313	309
	333		349
493	493	445	430
	B_{2g}		
		84	
109		113	101
170	149	157	165
			195
308	309	302	283
	450	445	342
481	484	460	394
611	609	511	539
	B_{3g}		
		100	156
		221	182
		286	266
		435	360
		554	570
	B_{1g}		
		129	167
		167	207
		211	312
		271	405
		478	551

[a]Reference 17(a).
[b]Reference 17(b).
[c]Reference 24.

elastic constants available for $LaMnO_3$. Therefore, the values of the other elastic constants are presented without any comparison.

C. Phonon density of states

The computed phonon density of states obtained by using Eq. (2) for $LaMnO_3$, as shown in Fig. 1, spans the spectral range from 0 to 70 meV and shows no band gaps. The density of states shows a broad structure in 20–40 meV range with peaks around 9, 48, and 60 meV. The calculated partial densities of states (as shown in Fig. 1) for the La atoms show an energy distribution extending only up to 30 meV, while the phonon vibrations due to the Mn and O atoms contribute in the entire 70 meV range. Mn largely contributes only up to 40 meV. The peak around 9 meV is due to the La vibrations, whereas the peak at 48 and 60 meV can be attributed to those from the O ions.

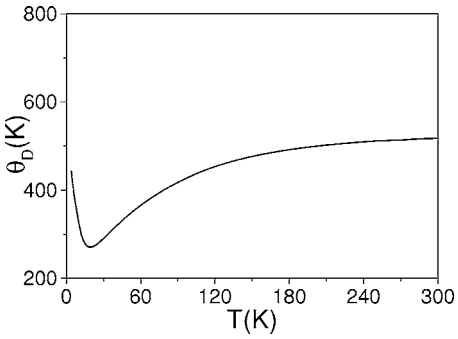

FIG. 4. The variation of Debye temperature with temperature as obtained from lattice dynamical calculations.

D. Raman and infrared results

We have depicted the results of group-theoretical analysis for the Γ-point phonons (Raman-active only) of orthorhombic $LaMnO_3$ (space-group *Pnma*) in Table III. Further, the calculated long-wavelength vibrational frequencies are compared with the available Raman[17(a),17(b)] spectroscopic data. The Raman lines of B_{1g} and B_{3g} symmetries (at 184 and 320 cm^{-1}), as reported in Ref. 17(a), are not unambiguous; hence, we have not shown them in Table III. In any case, the calculated phonon frequencies are in reasonably good agreement with the observed Raman[17(a),17(b)] data except for the highest frequencies, emphasizing the conjecture that ionic interactions play a major role in determining the vibrational properties too. A comparison to a shell model computation by Nikiforov and Popov[24] shows that the average deviation of the calculated Raman frequencies is 10.5%, whereas our present model gives this value as 7%. Further, they have used a much more complex model[24] with 20 parameters while our model has only 7 parameters. The present shell model has depicted all 24 Raman-active modes ($7A_g+5B_{1g}+7B_{2g}+5B_{3g}$) of vibrations and compared them with experimental[17(a),17(b)] and other shell model results.

The results on the 25 IR frequencies ($9B_{1u}+7B_{2u}+9B_{3u}$) calculated from the present shell model (along with the LO-TO splittings) are shown in Fig. 2. As the infrared measurements as reported in Ref. 18(a) were performed on twinned samples, they were not assigned to any symmetry. Further, we have presented the eight silent (A_u) modes of vibration in Fig. 2.

E. Specific heat

Lattice dynamical calculations yield C_V, the specific heat at constant volume. The experimental heat-capacity data correspond to C_P, the specific heat at constant pressure. The difference (due to the anharmonic lattice contribution)

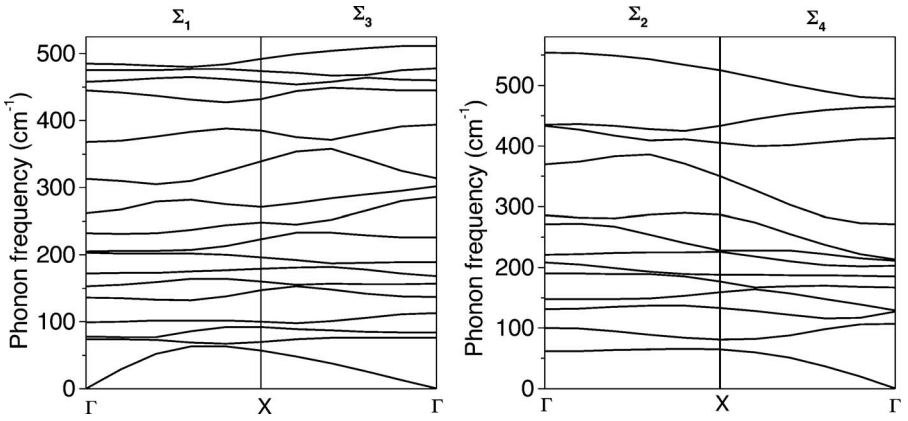

FIG. 5. Computed phonon-dispersion curves for $LaMnO_3$ along the high-symmetry Σ direction. Group-theoretical representations are indicated on top of the figure. Γ is the Brillouin-zone center and X is the zone boundary (1 meV=8.059 cm^{-1}=0.242 THz).

C_P-C_V=α_V^2 BVT, where α_V is the volume thermal expansion and B is the bulk modulus defined as $B=-VdP/dV$. In the Grüneisen approximation, all the phonon modes in the Brillouin zone are assumed to be characterized by $\bar{\Gamma}$, an average Grüneisen constant. The volume thermal-expansion coefficient is given by

$$\alpha_V(T) = \frac{\bar{\Gamma} C_V(T)}{BV_0}. \quad (4)$$

The calculated specific heat (as illustrated in Fig. 3) is higher than the available experimental values[16(a),16(b)] in the temperature range $70 \leqslant T \leqslant 600$ K. The anharmonic lattice contribution to the specific heat is computed to be around 3.5% around 300 K. $LaMnO_3$ undergoes a paramagnetic-to-ferromagnetic transition at 126 K; this is seen as a peak in the specific heat. Since our computations take account of only the phonon contribution to the specific heat, this peak is not reproduced in our calculations. We have also calculated the Debye temperature (as shown in Fig. 4), and it varies from 270 to 515 K in the temperature range of up to 300 K. In the low-temperature region (of up to 10 K), this calculated variation is in the range 300–445 K; this is in fair agreement with the reported experimental values of 305 K (Ref. 38) and 369 K (Ref. 39) deduced from specific-heat measurements up to 10 K.

F. Phonon-dispersion curves

The theoretically calculated phonon-dispersion curves for $LaMnO_3$ along the three high-symmetry directions Σ, Δ, and Λ in the Brillouin zone are shown in Figs. 5–7. The modes that belong to different representations are plotted separately in the same figures. Since there are 20 atoms in the unit cell, there are 60 phonon branches along each direction. At zone boundary points X, Y, and Z, the branches degenerate in pairs due to the high symmetry at these points. Along all the three directions, the branches are distributed uniformly up to 500 cm^{-1}.

V. CONCLUSIONS

On the basis of the above discussions, it may be concluded that the present simple and improved shell-model[23] approach for $LaMnO_3$ reveals the structural, vibrational, and thermodynamical properties of lanthanum manganite fairly accurately. This conclusion implies that the interatomic interactions in this manganite are predominantly ionic. Hence, the

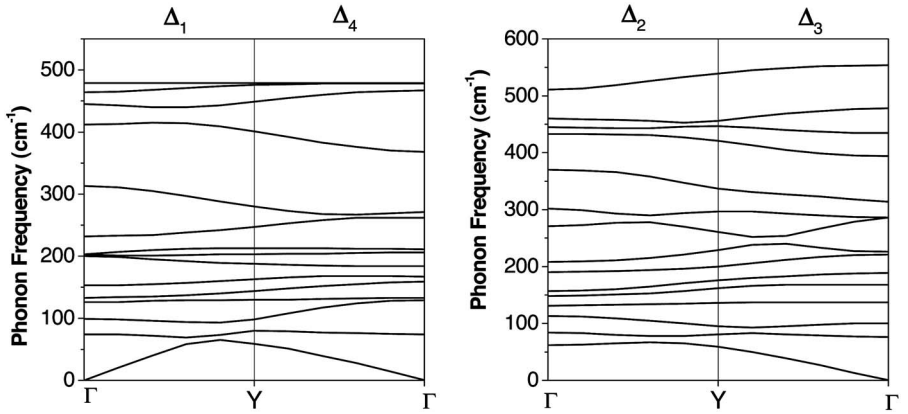

FIG. 6. Computed phonon-dispersion curves for $LaMnO_3$ along the high-symmetry Δ direction. Group-theoretical representations are indicated on top of the figure. Γ is the Brillouin-zone center and Y is the zone boundary (1 meV=8.059 cm^{-1}=0.242 THz).

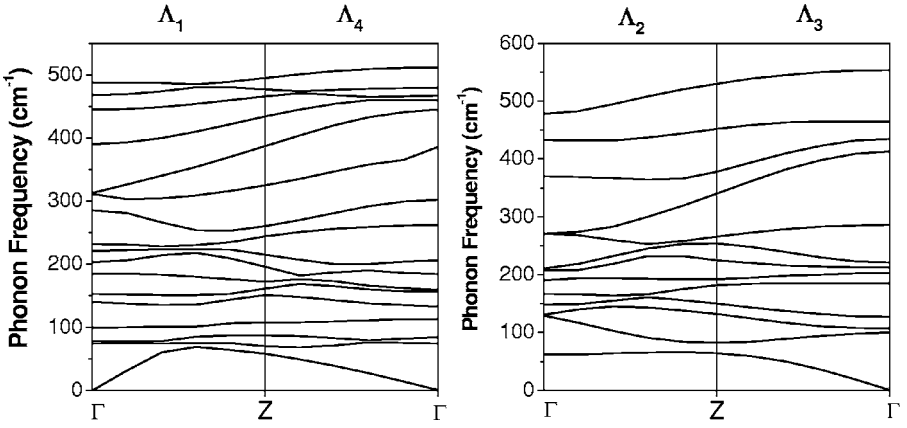

FIG. 7. Computed phonon-dispersion curves for $LaMnO_3$ along the high-symmetry Λ direction. Group-theoretical representations are indicated on top of the figure. Γ is the Brillouin-zone center and Z is the zone boundary (1 meV=8.059 cm^{-1}=0.242 THz).

model has the potential to describe the properties of other similar manganites. Also, the information about optical phonons may greatly help in further studies of the doping and temperature dependence of the phonon modes in $La_{1-x}A_xMnO_3$ (A=Ca, Sr, Br) and of their interplay with the magnetoresistance effect. The group-theoretical analysis of the phonon frequencies and polarization vectors at the zone center (Γ) point has been used for the interpretation of the Raman[17(a),17(b)] and infrared spectra[18] in $LaMnO_3$ (*Pnma* phase). Finally, it may be mentioned that the present results on the elastic constants and the phonon-dispersion curves are being reported, probably for the first time and hence they may serve as a guide to the experimental workers, in future.

ACKNOWLEDGMENTS

E.G.R. is thankful to the University Grants Commission (UGC) and the Council of Scientific and Industrial Research for financial support, and to M.P. Verma and Vilas Shelke, Department of Physics, Barkatullah University, Bhopal, for useful discussions.

[1] R. von Helmolt, J. Wecker, B. Holzapfel, L. Schultz, and K. Samwer, Phys. Rev. Lett. **71**, 2331 (1993).
[2] P. Schiffer, A. P. Ramirez, W. Bao, and S. W. Cheong, Phys. Rev. Lett. **75**, 3336 (1995).
[3] C. N. R. Rao, J. Mater. Chem. **9**, 1 (1999).
[4] S. Jin, T. H. Tiefel, M. McCormack, R. A. Fastnacht, R. Ramesh, and L. H. Chen, Science **264**, 413 (1994).
[5] K. Petrov, L. Krusin-Elbaum, J. Z. Sun, O. Field, and P. R. Duncombe, Appl. Phys. Lett. **75**, 995 (1999).
[6] J. Z. Sun, L. Krusin-Elbaum, A. Gupta, G. Xiao, P. R. Duncombe, and S. S. P. Parkin, IBM J. Res. Dev. **42**, 89 (1998).
[7] S. S. P. Parkin, Annu. Rev. Mater. Sci. **25**, 357 (1995).
[8] N. Furukawa, J. Phys. Soc. Jpn. **63**, 3214 (1994).
[9] J. B. A. A. Elemans, B. V. Larr, K. R. V. D. Veen, and B. O. Looptra, J. Solid State Chem. **3**, 238 (1971).
[10] B. C. Tofield and W. R. Scott, J. Solid State Chem. **10**, 183 (1974).
[11] J. A. M. van Roosmalen and E. H. P. Cordfunke, J. Solid State Chem. **110**, 106 (1994).
[12] P. Norby, I. G. Krogh Andersen, E. Krogh Andersen, and N. H. Andersen, J. Solid State Chem. **119**, 191 (1995).
[13] J. F. Mitchell, D. N. Argyriou, C. D. Potter, D. G. Hinks, J. D. Jorgensen, and S. D. Bader, Phys. Rev. B **54**, 6172 (1996).
[14] Q. Huang, A. Santoro, J. W. Lynn, R. W. Erwin, J. A. Borchers, J. L. Peng, and R. L. Greene, Phys. Rev. B **55**, 14987 (1997).
[15] J. Rodriguez-Carvajal, M. Hennion, F. Moussa, A. H. Moudden, L. Pinsard, and A. Revcolevschi, Phys. Rev. B **57**, R3189 (1998).
[16] (a) A. Michalopoulou, C. Papastaicoudis, and E. Syskakis, Physica B **284**, 1412 (2000); (b) H. Satoh, M. Takagi, K. Kinukawa, and N. Kamegashira, Thermochim. Acta **299**, 123 (1997).
[17] (a) M. N. Iliev, M. V. Abrashev, H. G. Lee, V. N. Popov, Y. Y. Sun, C. Thomsen, R. L. Meng, and C. W. Chu, Phys. Rev. B **57**, 2872 (1998); (b) V. B. Podobedov, A. Weber, D. B. Romero, J. P. Rice, and H. D. Drew, Phys. Rev. B **58**, 43 (1998).
[18] (a) A. Paolone, P. Roy, A. Pimenov, A. Loidl, O. K. Melnikov, and A. Ya. Shapiro, Phys. Rev. B **61**, 11255 (2000); (b) I. Fedorov, J. Lorenzana, P. Dore, G. De Marzi, P. Maselli, P. Calvani, S.-W. Cheong, S. Koval, and R. Migoni, *ibid.* **60**, 11875 (1999).
[19] T. Goto, T. Kimura, G. Lawes, A. P. Ramirez, and Y. Tokura, Phys. Rev. Lett. **92**, 257201 (2004).
[20] M. N. Iliev, M. V. Abrashev, J. Laverdiere, S. Jandl, M. M. Gospodinov, Y. Q. Wang, and Y. Y. Sun, Phys. Rev. B **73**, 064302 (2006).
[21] F. L. Tang and X. Zhang, Phys. Rev. B **73**, 144401 (2006).
[22] J. Baier, D. Meier, K. Berggold, J. Hemberger, A. Balbashov, J. A. Mydosh, and T. Lorenz, Phys. Rev. B **73**, 100402(R) (2006).
[23] Mala N. Rao, S. L. Chaplot, N. Choudhury, K. R. Rao, R. T. Azuah, W. T. Montfrooij, and S. M. Bennington, Phys. Rev. B **60**, 12061 (1999).
[24] A. E. Nikiforov and S. E. Popov, Phys. Solid State **43**, 1132 (2001).

[25] I. S. Smirnova, Physica B **262**, 247 (1999).
[26] M. N. Iliev, H. G. Lee, V. N. Popov, M. V. Abrashev, A. Hamed, R. L. Meng, and C. W. Chu, Phys. Rev. B **56**, 2488 (1997); V. N. Popov, J. Phys.: Condens. Matter **7**, 1625 (1995).
[27] E. Granado, N. O. Moreno, A. Garcia, J. A. Sanjurjo, C. Rettori, I. Torriani, S. B. Oseroff, J. J. Neumeier, K. J. McClellan, S.-W. Cheong, and Y. Tokura, Phys. Rev. B **58**, 11435 (1998).
[28] R. K. Singh, N. K. Gaur, and S. L. Chaplot, Phys. Rev. B **35**, 4462 (1987).
[29] R. K. Singh, N. K. Gaur, and S. L. Chaplot, Phys. Rev. B **36**, 5047 (1987).
[30] R. K. Singh and S. L. Chaplot, Phys. Status Solidi B **112**, 717 (1982).
[31] R. K. Singh, N. K. Gaur, and S. L. Chaplot, Phys. Rev. B **37**, 3089 (1988).
[32] S. L. Chaplot, N. Choudhury, Subrata Ghose, Mala N. Rao, R. Mittal, and P. Goel, Eur. J. Mineral. **14**, 291 (2002); S. L. Chaplot, Bhabha Atomic Research Centre, External Report No. BARC-972, 1978 (unpublished).
[33] N. Choudhury, S. L. Chaplot, and K. R. Rao, Phys. Chem. Miner. **16**, 599 (1989).
[34] K. R. Rao, S. L. Chaplot, N. Choudhury, S. Ghose, J. M. Hastings, L. M. Corliss, and D. L. Price, Phys. Chem. Miner. **16**, 83 (1988).
[35] With these potential parameters, the maximum force on any atom is less than 0.006 eV/Å. This order of the force is considered as "vanishing."
[36] (a) S. L. Chaplot, Phys. Rev. B **37**, 7435 (1988); (b) S. L. Chaplot, N. Choudhury, and K. R. Rao, Am. Mineral. **83**, 937 (1998); (c) A. Sen, S. L. Chaplot, and R. Mittal, Phys. Rev. B **64**, 024304 (2001).
[37] M. Saint-Paul and P. Lejay, Physica B **352**, 353 (2004).
[38] B. F. Woodfield, M. L. Wilson, and J. M. Byers, Phys. Rev. Lett. **78**, 3201 (1997).
[39] L. Ghivelder, I. A. Castillo, M. A. Gusmao, J. A. Alonso, and L. F. Cohen, Phys. Rev. B **60**, 12184 (1999).